Appl. Phys. B 71, 33–41 (2000) / Digital Object Identifier (DOI) 10.1007/s003400000238

Applied Physics B
Lasers
and Optics

Effect of various ions on organic light-emitting diodes obtained by ion-beam-assisted deposition

R. Antony, A. Moliton, B. Ratier

Unité de Microélectronique, Optoélectronique et Polymères (U.M.O.P., EA 1072), Faculté des Sciences, 123 av. Albert Thomas, 87060 Limoges cedex, France

Received: 13 September 1999/Revised version: 14 December 1999/Published online: 7 June 2000 –

Abstract. We present new optoelectronic results upon realization of organic light-emitting diodes obtained in sandwiched structures (ITO/Alq3/Ca/Al) with an original method for organic (Alq3) thin film deposition: the ion-beam-assisted deposition (IBAD). We compare the effects of various ion types: inert ions such as helium and argon, chemically active ions such as iodine (halogens that can act as a P doping in organic materials). We demonstrate that helium ion-beam assistance ($E = 100\,\text{eV},\ j = 100\,\text{nA/cm}^2$) realized on the anode side leads to enhanced luminance and quantum efficiency (ten times higher with respect to virgin layer) whereas argon always produces bad effects. Iodine ion beam also induces beneficial effects we attribute to an improvement of the hole injection and to an increase of the P-type conductivity.

PACS: 81.15.Hi; 85.60.Jb; 42.70.Jk

In recent years, numerous studies have been realized in the field of organic light-emitting diodes because their potential application to flat-panel displays [1–3]. Usually, the device structure consists of a luminescent layer sandwiched between charge-injecting electrodes. In order to increase the internal quantum efficiency, some authors have inserted hole and electron transporting layers between the two metallic contacts and the organic layer [4–6]. With these multilayer structures, the optoelectronic properties of the devices are improved.

Recently we have realized light-emitting diodes with a deposition process only used with the inorganic materials until now (ion-beam-assisted deposition: IBAD) [7]. Initially, we used an iodine ion-beam in order to assist the organic layer deposition; then we obtained a tenfold improvement in efficiency [8]. As a function of the ion types: helium, argon, and iodine ions (which exhibit various ion masses and various chemical properties), we present in this paper new optoelectronic properties obtained with this process (IBAD).

1 Experimental

The organic light-emitting diodes have a typical sandwiched structure (Fig. 1). For efficient electron injection, a low-work-function metal (2.9 eV with calcium) is used at the cathode, whereas the substrate is an indium-tin-oxide (ITO)-coated glass allocating a high work-function (4.6 eV with ITO) to the anode. The ITO layer is approximately 300 nm in thickness and its squared resistance is 4 Ω/□. The calcium cathode is realized by physical vapor deposition under a secondary vacuum; in order to prevent a possible oxidation, an aluminium layer is deposited on the top of this calcium layer. Calcium and aluminium films have, respectively, 200 nm and 100 nm in thickness; the mask used for the calcium evaporation determines the light-emitting diode size (4 mm^2). The organic luminescent material is a fluorescent chelate complex: the tris (8-hydroxyquinoline) aluminium (Alq3) with a band gap around 2.4 eV and an ionization potential equal to 5.9 eV [9]. Many authors have used this molecular material in order to obtain a green-color light from emitting structures [1, 10]. The weak molecular weight of the Alq3 allows a deposition by thermal evaporation we realized under a secondary vacuum (10^{-6} mbar); the thickness of the deposited layer (75 nm) is accurately determined with a quartz balance.

The IBAD system combines simultaneously vapor film deposition and bombardment with an independently controlled ion-beam: Fig. 2. The boat used for the thermal deposition is laid in a perpendicular direction to the substrate and the angle between the evaporated beam and the ion-beam is 45°. This ion-beam is produced by a low-energy accelera-

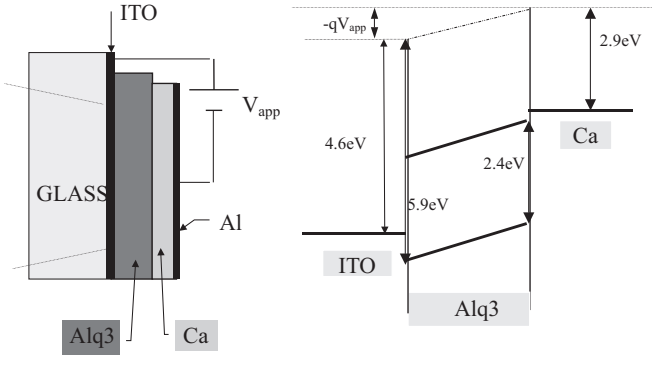

Fig. 1. Structure of an ITO/Alq3/Ca/Al light emitting diode

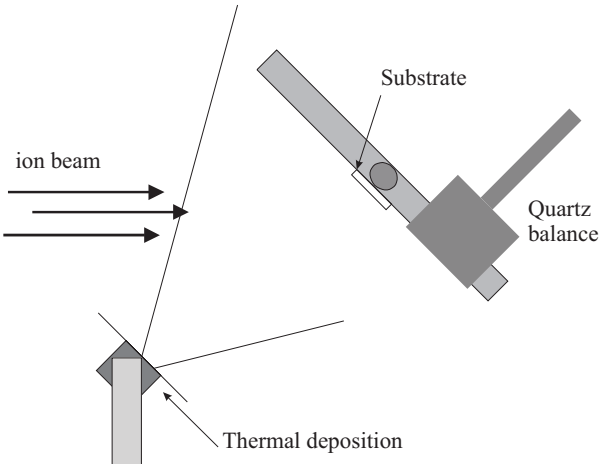

Fig. 2. Scheme of the ion-beam-assisted deposition system

tor (Fig. 3a) with a similar configuration to the one described elsewhere [11]. As for us, to obtain low ion energy with a sufficiently high current density, we utilized an electron cyclotron resonance (ECR) source brought up to a voltage that determines the ion energy; the basic theory of such an ion source is based on the resonance condition which assumes the energy transfer between the electromagnetic field and electron: this occurs when the electron undergoes precisely one circular orbit in one period of the applied field [12]; the electromagnetic field is produced by a 10-GHz microwave generator and the magnetic field (3500 Gauss) required to obtain the resonance condition is delivered by permanent magnets [13]. With supply voltages of the beam transport components described in Fig. 3b, we finally obtain in the chamber a uniform parallel beam with ion energy contained between 10 eV and 30 keV and a current density as high as $100\,\mathrm{nA/cm^2}$ we measured with a Faraday cup. More precisely, this uniform and parallel beam with selected ions is obtained by way of a $\mathrm{E} \times \mathrm{B}$ mass separator (Wien filter), a neutral beam trap, and a double-*XY* sweeping system; a decelerating lens allows operation in the wide energy range 10–30 keV; the sputtering of this lens is limited by its geometrical shape (cylinder coaxial with the parallel ion-beam so that the ion-beam cannot collide with the lens significantly). The ions used for this study are helium, argon, and iodine; the first two are chemically inactive and they do not affect the organic material conductivity, whereas iodine is considered as a P-type doping ion. Thus, it can induce an electrical property modification of the Alq3 considered as a N-type material.

Various optoelectronic characterizations are realized on the electroluminescent structures. The emission spectra are measured with a Zeiss MQ3 monochromator coupled with a Hamamatsu photomultiplicator (R-636 type) with a flat spectral response on a large wavelength scale (300–800 nm). The dark current, luminance, and internal quantum efficiency measurements are obtained with a large-area photodiode ($100\,\mathrm{mm^2}$) coupled with a Keithley 175 multimeter and with a Keithley 617 electrometer. All optoelectronic characterizations are realized under a primary vacuum (6×10^{-1} mbar) in order to prevent the calcium oxidation.

2 Computer simulation of stopping power and sputtering yield of helium, argon, and iodine ions in Alq3; expected effects of the IBAD process

2.1 Computer simulation

The general trend in IBAD is to use a low-energy ion beam in the 50–500 eV range. In this energy range nuclear stopping power (involving elastic collisions) is assumed to play the major contribution in energy transfer between the impinging

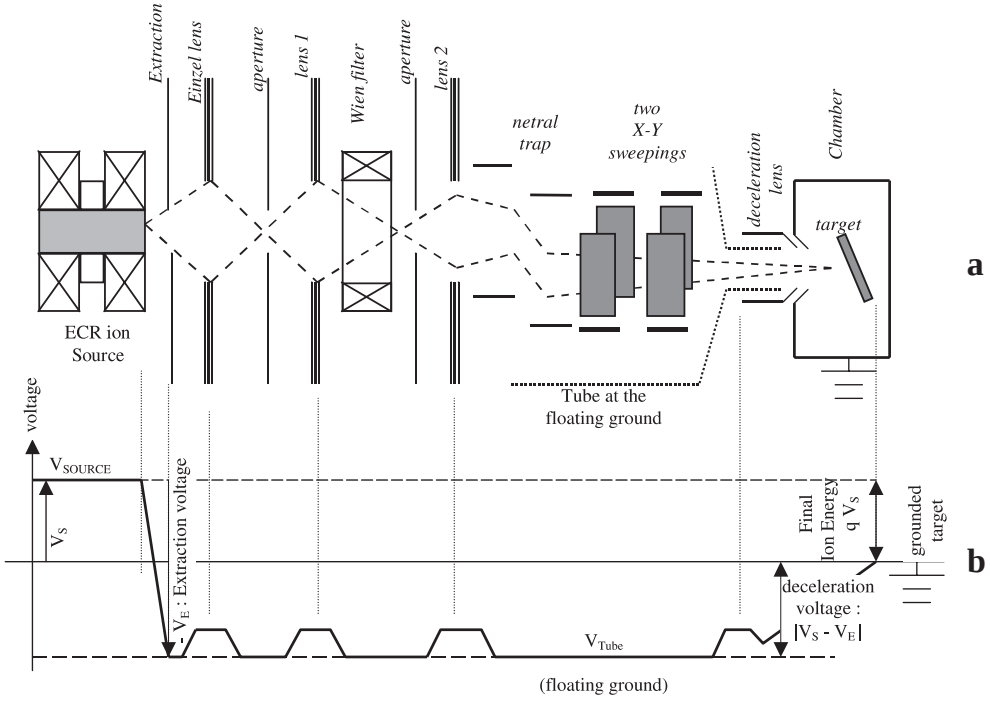

Fig. 3. a Main components of the ion-beam system. **b** Supply voltages of the beam transport components (the beam voltage is typically $V_\mathrm{E} = 20$ kV)

ions and the atoms of the target, so that sputtering of the target atoms is unlikely to be neglected. According to Smidt [14] a sputtering yield (number of atoms ejected from the surface per incident ion) lower than 1 atom/ion is desirable in order to prevent the film growth-rate limitation.

So a computer simulation of the sputtering yield of helium, argon, and iodine ions in Alq3 was carried out with the Monte Carlo program SRIM2000, a new version of TRIM [15]. This program is based on the binary collision approximation (BCA) and is suitable to explain the main phenomena involved in the ion–target interaction (recoils, replacements, and vacancies of atoms, phonon distribution, ion backscattering) provided the ion energy is not lower than 100 eV (for lower energies the BCA breaks down due to multiparticle interactions [16, 17]). The energy range of the incident ions was varying from 100 eV to 30 keV and the incidence angle of the ion-beam was 45° in order to respect the experimental configuration. Each sputtering yield for a given ion energy was determined with a 2000-incident-ion averaging.

Figures 4 and 5 show the sputtering yield and the stopping powers of the three above-mentioned ions versus ion energy. Since the binary collision process is mainly dependent on the ion/atom mass ratio, preferential sputtering occurs in the case of a polyatomic target. In the case of Alq3 the higher sputtering yield is obtained for the carbon atoms (although hydrogen sputtering was not negligible in the case of 100-eV helium ions). Only sputtering yields of carbon atoms are presented in Fig. 4 for better clarity. Since higher energies give too high a sputtering yield (higher than 1) for IBAD process, the energy range presented in this figure is limited from 100 eV to 5 keV.

As expected, the same trends in amplitude and shape of the two sets of curves clearly demonstrate that sputtering yield is mainly governed by the nuclear stopping power of ions in the material. The crossing point of both argon and iodine stopping power and sputtering yield curves below the keV range (due to the reduced mass effect [15], the maximum nuclear stopping power happens at a higher energy for a higher ion–atom mass ratio) can be pointed out, so that for the lowest energies the sputtering yield of iodine will be unambiguously lower than the argon one (1.5×10^{-3} and

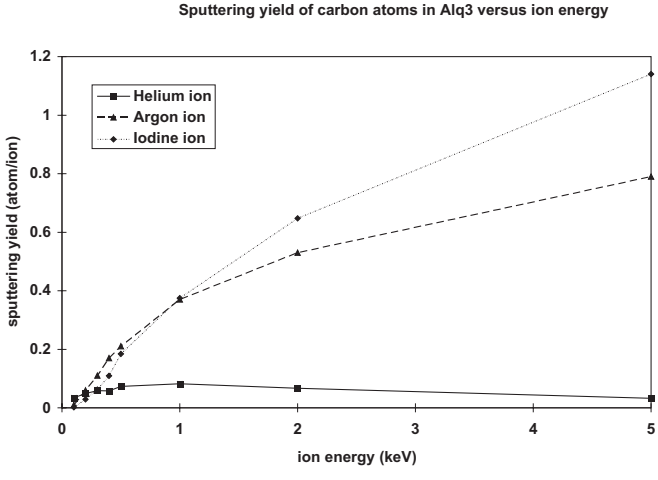

Fig. 4. Sputtering yield of carbon atoms in Alq3 versus ion energy for helium, argon, and iodine ions

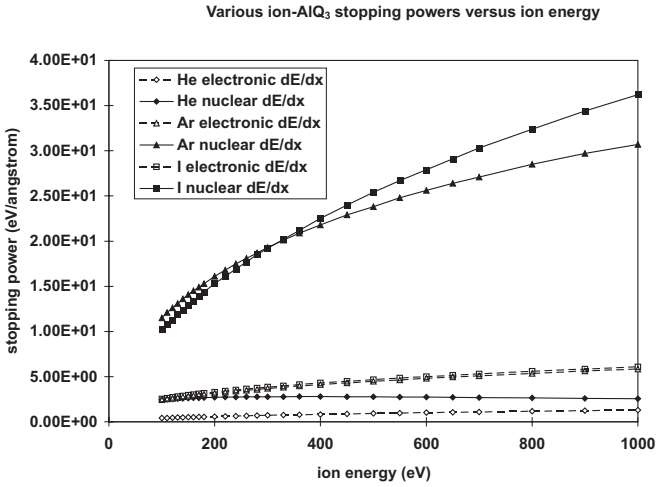

Fig. 5. Stopping powers of helium, argon, and iodine ions versus ion energy in Alq3

10^{-2} atom/ion at 100 eV, respectively). Obviously the sputtering yield amplitude of both ions forbids their use for IBAD process at energies above 500 eV. For the helium ions, which present a low ion/atom mass ratio, the sputtering yield remains low for the whole energy range and would not be a cause of limitation of the IBAD process. Moreover these latter sputtering yields must be seriously minimized because of the great amount of backscattered helium ions at low energy (around 20% at 100 eV whereas no noteworthy backscattering was noticed in the case of argon and iodine ions).

On the other hand these simulations do not take into account any chemical effect of the ions and the BCA model treats only ion–atom collisions. These results only give an energy domain where the IBAD process can be used.

2.2 Expected effects of the IBAD process

To improve organic light-emitting diodes (OLEDs), generally a multilayer structure is built in order to increase hole–electron recombinations. In our case, as Alq3 is an ETL (electron transport layer), a HTL (hole transport layer) is deposited on the anode side for hole injection. Until then, a chemical way was used to realize HTL [10]: for example, a layer of TPD (tetraphenyldiamine) or of P3OT (poly-3-octylthiophene, which is a P-type conducting polymer) can be deposited on the anode side.

In a novel way, we have studied a physical way based on the ion-beam effects to reinforce carrier injection and hole–electron recombination. The first results obtained in our laboratory with the IBAD technique and iodine ions have shown beneficial effects on the Alq3 electroluminescent properties [8, 18]. For this present study, we have assisted the organic material deposition on different thickness with various ion types. The geometrical origin of the layers is taken on the top of the ITO layer and as described in Fig. 6, we consider three areas: 0–25 nm (area 1), 25–50 nm (area 2), 50–75 nm (area 3), each of them being "assisted" or "non-assisted" as mentioned below for each experiment. Nevertheless, the Alq3 deposition is continuously realized ("assisted" layer and "non-assisted" [or virgin] layer) in the chamber until the desired final thickness (75 nm) is reached (in order

to avoid the interface effects between the "assisted" and the "virgin" layer). On the various curves we shall present, the meaning of the captions is as follow:

* $0 \rightarrow 25$ nm: sample (structure [1]) obtained with assistance on area 1 (0–25 nm), while areas 2 and 3 are unassisted.
* $0 \rightarrow 50$ nm: sample (structure [2]) obtained with assistance on areas 1 and 2 (0–25 nm and 25–50 nm, that is to say 0–50 nm) while area 3 is unassisted.
* $0 \rightarrow 75$ nm: sample (structure [3]) obtained with assistance on areas 1, 2, and 3 (0–25 nm, 25–50 nm, and 50–75 nm, that is to say 0–75 nm).

First time, the ion-beam parameters are chosen from the laboratory experience in the field of the ion-beam process and in agreement with the energy selected by Kyokane et al. [19, 20]; typically we used: ion energy $E_i = 100$ eV, ion-beam current density $J_i = 100\,\text{nA/cm}^2$, assistance duration $t = 120$ s. In the last section, we will present results as a function of the ion-energy which will justify this preliminary ion-energy choice.

With regard to the specific film properties generated by deposited ions we can consider they are issued from the following competitive effects:

– Effect 1: Effect of ion bombardment on nucleation and early stages of growth of thin films [14], which is an interface (ITO/Alq3) effect; there are not clearly defined trends since in some cases nucleation is enhanced and island size decreases, and in some cases the number of nuclei is reduced and island growth is accelerated. In fact, enhanced adatom mobility is frequently cited as a factor in IBAD that would influence nucleation and growth processes. As a result, we can consider we obtain a limitation of the porosity number at the interface between the substrate (ITO in our case) and the deposited film with an increase of the specific surface between the substrate and the film: an enhancement of the hole injection is then expected at the ITO anode.
– Effect 2: Effect of ion-beam-assisted deposition on microstructure of thin films [14] which is a bulk effect; microstructural modifications produced by IBAD is the densification of zone 1 (associated with numerous porosities in the Movchan and Demchishin [21] representation) of the Thornton model [22], as a result of knock-on atoms filling the voids (modeling of Muller [23]). The structural effect (with an enhancement of the volume densification) on the resistivity results from the general decrease in grain size for bombardment-modified films: due to increased scattering at grain boundaries, the resulting resistivity is generally increased [24].
– Effects 3: Following the interactions ions – substrate, two defect types can appear:
  • 3a: Bond breakdowns can be produced inside the layer with generation of dangling bonds which can act as non-radiative recombination centers (the luminescence is then quenched as we demonstrate during ion implantation of conducting polymers [25]); furthermore, dangling bonds [26] can be associated with localized states: in the vicinity of the cathode, these states can trap electrons and reduce their injection.
  • 3b: Incoming ions can be trapped inside the layer and then act as exciton traps.
– Effect 4: Electrical dopping with a reinforcement of the current density produced by charge transfer between interstitial ions (akali or halogen) and organic molecules (or polymers) [27].
– Effect 5: Optical dopping generated by ions with specific optical properties (such as lanthanides [28] which can emit in the infrared (erbium), in the red (europium), in the green (terbium)...).

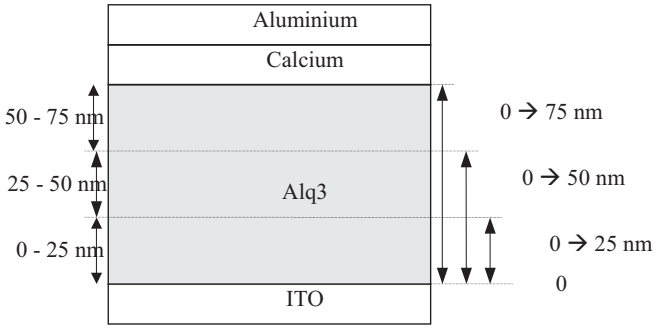

Fig. 6. Scheme of the various assisted zones (virgin sample is obtained without assistance on the whole thickness); structure 1 is obtained with assistance on the area $0 \rightarrow 25$ nm; structure 2 is obtained with assistance on the area $0 \rightarrow 50$ nm; structure 3 is obtained with assistance on the area $0 \rightarrow 75$ nm

3 Results at a given energy (100 eV) and discussion

3.1 IBAD with a helium-ion beam

The layout of the electroluminescence spectra with different structures shows that the use of a helium-ion beam in order to assist the luminescent layer deposition has no sensitive influence on the wavelength emission (Fig. 7) and is unconnected with the assisted zone thickness: the emitted light is clearly visible and always exhibits a green color (λ_{max} changes between 530 and 550 nm). The structure obtained with an ion-beam assistance on the whole thickness ($0 \rightarrow 75$ nm) does not produce enough luminance to be detected by the photomultiplier after its crossing through the monochromator (and the spectrum is not drawn in Fig. 7). Finally, it seems therefore that the use of a helium ion-beam does not modify the Alq3 gap.

The variations of the dark current (I) as a function of the applied voltage (V) on the structures are shown on the inset of Fig. 8. We can observe that the use of an ion-beam to assist the Alq3 layer deposition induces a displacement of the threshold voltage and the structure seems to become more resistive. This evolution is all the more important as the assisted-zone thickness is great and can be well explained by effect 2 of the IBAD process; the current density governed by the majority carriers (electrons) decreases when the IBAD process is applied: then electron traps are probably generated in the ion-beam-assisted layer.

The layout of the $L = f(V)$ characteristics (L: luminance) of each structure demonstrates the helium ion-beam effect is very beneficial when the assisted zone is contained between 0 and 25 nm (Fig. 8): the luminance becomes five times higher than with the virgin structure. If the thickness

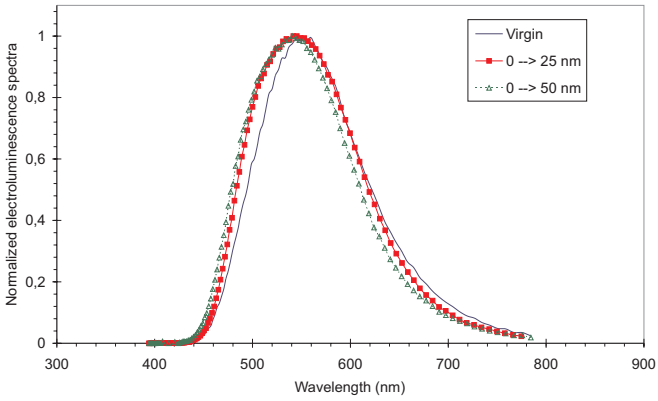

Fig. 7. Electroluminescence spectra of LEDs realized with helium IBAD

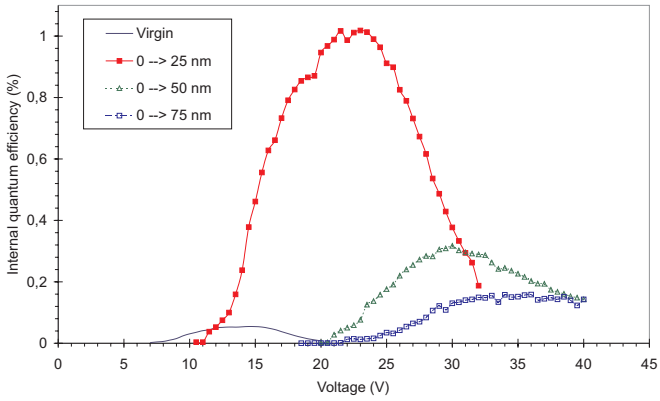

Fig. 9. $\eta = f(V)$ characteristics of LEDs realized with helium IBAD

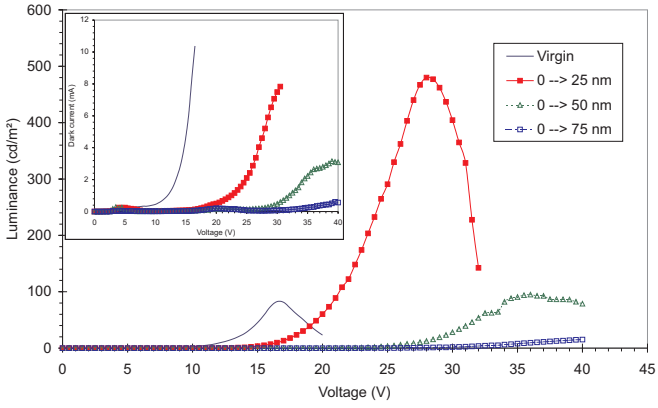

Fig. 8. $L = f(V)$ characteristics of LEDs realized with helium IBAD; *inset*: $I = f(V)$ characteristics

of the assisted zone increases, the luminance decreases and values obtained with a completely assisted Alq3 layer are weaker than those obtained with a virgin structure. So, in the case of structure 1 (assisted on the area $0 \rightarrow 25$ nm), we can think that effect 1 becomes predominant in relation to other effects with an increase of hole injection: as the minority carriers (holes in the present case) govern the radiative recombinations (that is to say exciton production) an enhancement of hole (minority carriers) injection induces a luminance increase.

On the contrary, the ion-beam has a negative effect on the luminance of structures obtained with a greater assisted thickness (structures 2 and 3); so, we can consider that effects 3 produced in the bulk of the film then becomes the most extensive, with too great a decrease of the current density associated with electrons (majority carriers): Figs. 8 and 9 of the 0–50 nm and 0–75 nm assisted structures. Nevertheless, effect 3b is limited by the helium-ion backscattering which becomes large because the helium-ion mass is small with respect to the Alq3 molecules.

Figure 9 shows the evolution of the internal quantum efficiency (η) according to the applied voltage. High efficiency improvement of the structure [1] in comparison with a virgin structure can be attributed to the positive effect 1 again. Another contribution to the quantum efficiency increase would be the generation of an electron confinement zone localized near the interface of the assisted–unassisted area, because the ion bombardment can induce a decrease of the electron mobility in the assisted zone. Indeed, the electron mobility can be estimated to a lower value in the assisted area insofar as we can assume that the IBAD process generates numerous electron traps located under the level E_c of the LUMO band (probably around 0.3 eV under E_c [10]): if n_t and n_f are the density of the trapped and of the free electrons, respectively, then the mobility is the effective mobility μ_{eff} with a same form as in the case of the TCL current (trapped charge-limitted current [8]): $\mu_{eff} = \theta_n \mu_f < \mu_f$, where μ_f is the mobility of the free electrons (without electron traps) and $\theta_n = (n_f/(n_t + n_f))$ so that $\theta_n < 1$. Finally a shift of the recombination zone towards the center of the OLED (comparable to a two-layer OLED) can be produced, with a recombination rate enhancement.

Furthermore, the quantum efficiency decreases as the thickness of the assisted zone increases: the hypothesis about the molecular material modifications (effect 3) can explain this quantum efficiency decreasing; moreover, too great a shift of the confinement area towards the cathode can also explain this decrease because the hole diffusion length (≈ 35 nm [10]) is too short to allow the holes to reach the confinement area (localized around 50 nm in the case of structure 2 because electrons are confined as soon as they reach the area of low mobility); in the case of structure 3 this confinement zone is nearly suppressed.

Finally, with respect to a structure obtained without assistance, this study with helium-ion-beam assistance of the emitting layer leads to enhanced optoelectronic properties when this assistance is confined to the first area (structure 1). It is interesting to note that the beneficial ion effect observed here (effect 1), is obtained in an indirect manner (modification at the interface of the Alq3 layer structure) because the direct ion effect (chemical ion effects: effect 4) cannot exist with these inert ions (helium). As a remark, we have verified that helium ion-beam treatment only located on the ITO anode does not produce a beneficial effect, so that we can affirm that beneficial effects actually occur near the interface during the deposition of the first helium-beam-assisted monolayers. A complementary hypothesis to the beneficial effect 1 could be to suppose that helium assistance just induces a suitable P-type character (defects inducing hole generation) which becomes modified with higher ion-beam parameter (energy, current density, ion size): numerous localized states then induce too low a mobility onductivity) [27].

3.2 IBAD with an argon-ion beam

Alq3 electroluminescent structures have now been realized with an ion-beam assistance with argon which is also a chemically inert element. However, because of its greater mass than helium, argon ions exhibit a decrease of the backscattering phenomenon as was noticed in Sect. 2; then there can appear inside the electroluminescent layer a more important number of trapped atoms or ions issued from the argon-beam assistance. Parameters of the ion beam are identical to those used with the helium-ion-beam ($E_i = 100$ eV, $J_i = 100\,\mathrm{nA/cm^2}$, $t = 120$ s) and this study is also realized according to the assisted-zone thickness.

Electroluminescence spectra of virgin and argon-ion-beam-assisted structures are similar: the spectrum shape remains the same with a peak close to 545 nm (Fig. 10). With the argon beam as well as with the helium beam, the gap of the luminescent material is not modified by the IBAD technique.

The inset of Fig. 11 shows the layout of the different $I = f(V)$ characteristics of the diodes with an increase of the resistivity as a function of the assisted thickness: with an ion-beam-assistance on the whole thickness (or on the area 0–50 nm), the value of the dark current is always lower than 10^{-4} A even when the applied electrical field is more than 10^8 V/m.

On Fig. 11 we notice that the argon-ion-beam-assistance is always prejudicial to the obtained luminances. Luminance of the structure 1 (assistance on the area 0–25 nm) is four times smaller than with a virgin structure; this very weak observed luminance (for structures 2 and 3, $L_{max} = 0.5\,\mathrm{cd/m^2}$ and $L_{max} = 0.25\,\mathrm{cd/m^2}$, respectively) proves that the radiative recombination number is strongly limited in relation to only negative effects induced by the argon-ion-beam:

* near the ITO interface, effect 1 is perhaps limited (Ar inclusions at the interface) with a decrease of the hole injection in argon-assisted layer.
* the negative effect 3 is very important with a reinforcement of the generation of defects (structural defects and also impurity defects associated with the low argon backscattering) that act as quenching sites inside the layers.

The comparative study of the internal quantum efficiency according to the inert ion mass (Fig. 12) follows the same reasoning. The efficiency obtained with a small-mass ion is close to 1%, whereas efficiency calculated with a greater ion mass is around the internal quantum efficiency of a virgin structure (0.06%, with an increase of the operating voltage in the case of argon-assisted deposition).

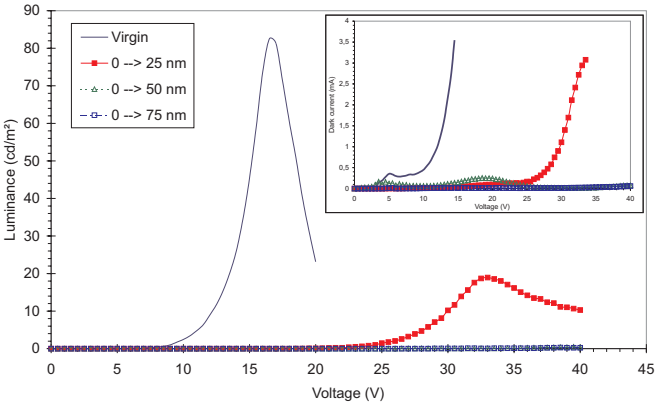

Fig. 11. $L = f(V)$ characteristics of LEDs realized with argon IBAD; *inset*: $I = f(V)$ characteristics

Finally, we can conclude that the use of an inert ion-beam in order to assist the luminescent material deposition has several effects according to the ion mass. Suitable inert ion-beams favor the Alq3 layer densification and hole injection with an improvement of luminance and internal quantum efficiency of the organic light-emitting diodes. Nevertheless, it is necessary to use this deposition technique with some precautions: extreme assistance parameters (ion mass is one of the most sensitive parameters) reduce the beneficial effects (effect 1) and enhance the resistivity (effect 2) as well as the negative effect (effect 3). Then the threshold voltage is increased and a diminution of the radiative recombination number is induced: the ion-beam effect on the luminescence becomes negative.

3.3 IBAD with an iodine ion-beam

The first experiments we realized by the IBAD technique were obtained with an iodine ion-beam [8, 18] and we showed that the assistance with a 100-eV iodine-ion energy leads to a tenfold improvement in internal quantum efficiency. Iodine

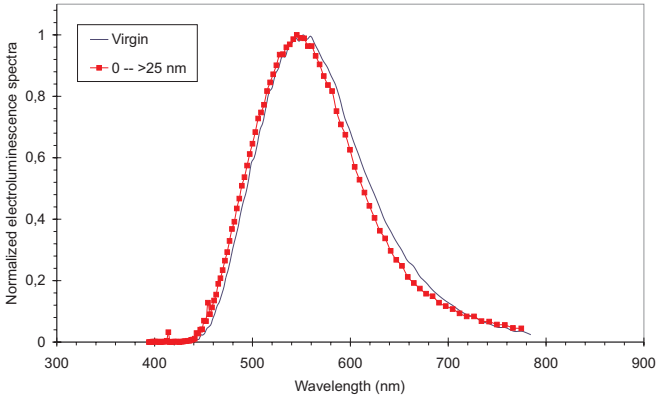

Fig. 10. Electroluminescence spectra of LEDs realized with argon IBAD

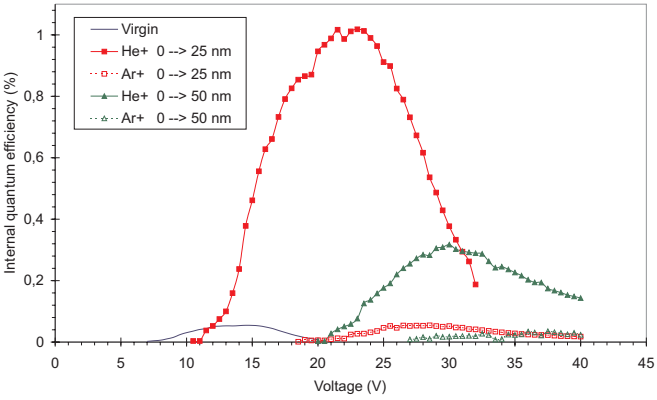

Fig. 12. Ion mass influence on the $\eta = f(V)$ characteristics

has an atomic mass three times greater than the argon and the previous study has allowed us to point out the influence of the ion mass on the Alq3 deposition. Nevertheless, the results obtained with iodine (which can also act as a P-type chemical doping) seems to contradict the results obtained with an argon-ion beam. This paradox can be easily explained by the SRIM2000 simulations: for a 100-eV ion-beam energy, the mean transferred energy to a carbon atom will be in the order of 30, 20, and 15 eV/atom for argon, helium, and iodine ions, respectively, so that damage caused by the argon beam are expected to be greater than those caused by the iodine beam. It may be also noticeable that this transferred energy will be of the same order for iodine and helium. So, with the aim of determining the influence of the ion doping effect, we now compare results obtained with helium ions and with iodine ions. Parameters of the ion-beam are the same as the optimum parameters used for the first study with iodine [8] ($E_i = 100$ eV, $J_i = 50\,\mathrm{nA/cm^2}$, $t = 60$ s), with the assisted zone contained between 25 and 50 nm (Fig. 6). As with chemically inert ions, the iodine ion beam does not modify the electroluminescence spectra significantly [8] and therefore it appears that the iodine doping character does not alter the Alq3 gap.

On the $I = f(V)$ characteristics, the displacement of the threshold voltage is observed with the two different ions; nevertheless, it is less important when the assistance is realized with an iodine ion-beam (Fig. 13). It seems therefore that the Alq3 layer deposited with an ion-beam exhibits various electrical properties according to whether the ion is chemically active or inert. With iodine, negative effects such as damage (effect 3a assumed to be of the same order as with helium ions) and also quenching traps (associated with numerous iodine inclusions due to a small iodine backscattering rate: effect 3b) can be compensated by another phenomenon linked to the doping character of the ion (effect 4) which induces an increase of the hole transport and an enhancement of the material conductivity.

The luminance obtained with the assistance of a helium ion-beam on the zone 25 to 50 nm is equal to $120\,\mathrm{cd/m^2}$, whereas the use of the iodine ion-beam allows us to double this result (Fig. 14). So, it is possible that the iodine ion-beam modifies the exciton distribution length in the Alq3, this value being estimated by Mori and Mizutani [30] to 20 nm in the virgin material. Furthermore, Burrows et al. [10] consider that the recovery of hole and electron densities is maximum at 30–40 nm in depth (area 30–40 nm) with a maximal number of generated excitons in this zone. Therefore, we think that radiative recombinations can be enhanced by two effects with iodine-ion assistance:

* a densification of the area 25–50 nm (effect 2) which then contains fewer traps (oxygen) which act as non-radiative centers;
* an increase of the hole number obtained by effect 4 (P-type chemical doping induced by iodine): in virgin Alq3, the weak hole number is one of the restrictive factors of the luminance.

The luminance is thus improved in comparison with an unassisted structure. The good results obtained with these structures indicate that the negative effects (influence of extinction sites linked to defects: iodine atoms inserted in the material, for example) are less extensive than the positive effects induced by the chemically active ion-beam; indeed, as Alq3 is a n-type layer (because aluminium atom withdraws the electrons of the ligands and increases the electron affinity as cyano substituent on the PPV chain [31]), iodine atoms located in interstitial sites can induce a P-type doping by charge transfer as explained during electrical doping of conducting polymers [27]: then the hole transport across the ion-beam-assisted layer is easier and the luminance as well as the internal quantum efficiency are improved.

So, the layout of the internal quantum efficiency of the structures shows that the assistance of the iodine ion-beam is beneficial (inset Fig. 14). The value of this parameter is multiplied by a factor 10 with halogens (0.6%) whereas the internal quantum efficiency of an assisted structure with the helium ion-beam on this zone is slightly weaker (0.45%); this result confirms the hypothesis formulated with the other optoelectronic characteristics.

4 Results versus ion energy

All these experiments have been made with an ion-beam energy of 100 eV according to the earlier works of Kyokane et al. [19, 20]. As mentioned in Sect. 2, ion–matter interaction strongly depends on the ion–atom mass ratio. Moreover the largest slopes of sputtering yield and nuclear stopping power versus energy curves occur below the keV range where IBAD process usually takes place. So a set of new experiments has been carried out versus ion beam energy in order to verify if the usual 100 eV is accurate.

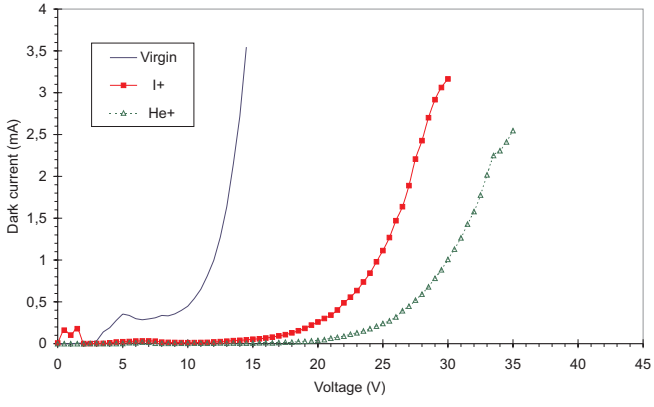

Fig. 13. Doping effects on the $I = f(V)$ characteristics

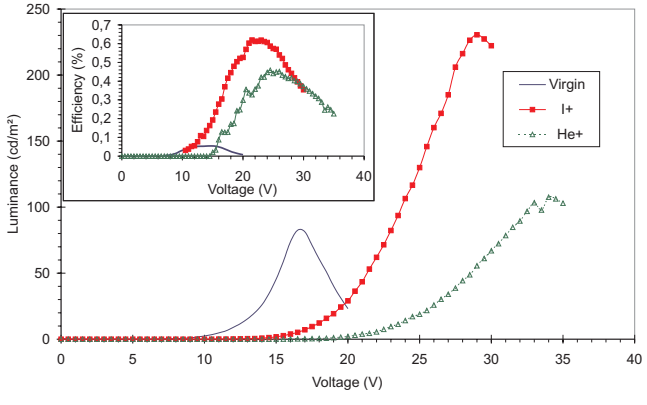

Fig. 14. Doping effects on the $L = f(V)$ characteristics; *inset*: $\eta = f(V)$ characteristics

In regard to the above results the assisted area was chosen according to the best optoelectronic characteristics obtained: 0–25 nm area for helium and argon ions and 25–50 nm for iodine ions. The ion-beam current density was 100 nA/cm^2 and the ion-beam energy were varying from 10 eV to 1 keV. (Elsewhere [32], experimentally we verified that the appropriate value of the current density must be contained between 50 and 100 nA/cm^2: outside this zone, optoelectronic parameters (L and η) become very small).

The maximum luminance and the maximum internal quantum efficiency of the diodes versus ion energy for the three ion types are presented in Fig. 15, where luminance (L) and quantum efficiency (η) for a non-assisted diode can be seen in dotted lines. These characteristics clearly show a maximum enhancement of the optoelectronic properties toward 100 eV in the case of helium and iodine ion-beam assistance and a decrease of this effect for the upper energy. The luminance obtained by IBAD with argon always remains lower than the one obtained with a non-assisted diode.

If on the one hand a continuous decrease (with the ion energy) of the optoelectronic properties of the diodes could be explained in terms of limitation by an increase of the energy transfer between ion and atoms, as it can be seen in Figs. 4 and 5, the presence of an optimum energy at 100 eV is not attempted on the other hand. At this energy the mean transferred energy to a carbon atom will be in the order of 20 eV/atom, that is to say the order of the replacement threshold of a target atom in matter, but could be important in the gas phase at the interface of the film growth. It is clear that many particle effects take place in this energy range and that molecular dynamics models are still lacking in explaining the phenomena involved during IBAD process [14].

5 Conclusion

Ion-beam-assisted deposition of Alq3 with various ion types demonstrates that optoelectronic properties results from the competition between beneficial effects and negative effects:

– beneficial effects are obtained with a helium-ion beam because the small ion-mass limits defect production whereas hole injection is reinforced with a sufficiently high mobility (and P-type conductivity) near the anode. Furthermore, an electron confinement layer located at the interface of the assisted–unassisted layer can be induced by the ion-beam (physical way), comparable to the one obtained by a chemical way in a two-layer OLED.
– with an iodine-ion beam, structural defect generation (iodine inclusions) is probably increased; however, the chemical effect of this halogen (electron acceptor which acts as P-type doping) can induce a hole injection increase with an improvement of the P-type conductivity: numerous excitons can be generated (around 25–50 nm) with better luminance and quantum efficiency.
– with an argon-ion beam, generated holes (in limited number because of the ion inert character) exhibit a very low mobility due to numerous defect production (bond breakings, atom inclusions): the P-type conductivity is very low and these defects act as quenching sites for the luminescence which becomes very small.

The use of the IBAD process with some ions allows us to improve the luminescent properties of Alq3 light-emitting diodes. This study shows that there are various effects according to the ion type and it seems interesting to realize ion-beam-assisted deposition with fluorine or chlorine in order to combine the two beneficial effects: small-ion-mass effect and the P-type-doping effect. In fact, our initial experiments with the iodine-ion beam have stopped because the ECR ion source has been damaged by the reactive halogen ions; now, a new ion source (hollow cathode) is progressing in order to obtain suitable current density (100 nA/cm^2) in the low-energy range (100 eV) with halogen and lanthanides (to study effect 5: optical doping). As soon as possible, a comparative study of organic light-emitting diodes obtained by ion-beam-assisted deposition with various halogen and lanthanide ions will be undertaken; then the important lifetime parameter will be studied also [33].

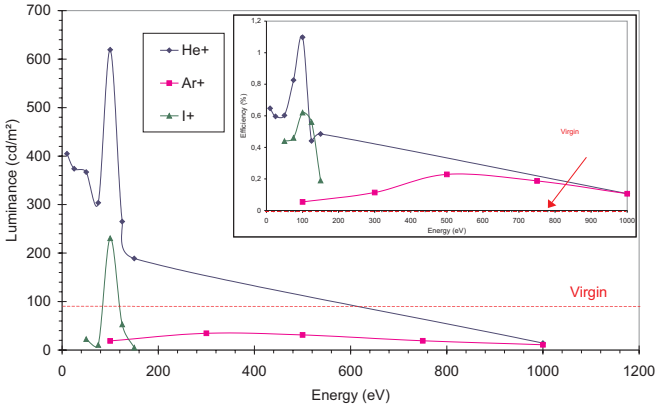

Fig. 15. Maximum luminance versus ion energy; *inset*: maximum internal quantum efficiency versus ion energy

References

1. C.W. Tang, S.A. VanSlyke: Appl. Phys. Lett. **51**, 913 (1987)
2. J.H. Burroughes, D.D.C. Bradley, A.R. Brown, R.N. Marks, K. Mackay, R.H. Friend, P.L. Burns, A.B. Holmes: Nature **347**, 539 (1990)
3. R.H. Friend, N.C. Greenham: *Handbook of Conducting Polymers*, 2nd edn., ed. by R. Elsenbaumer, J.R. Reynolds, T. Stokeim (Marcel Dekker, New York 1997) Chapt. 29
4. A.R. Brown, D.D.C. Bradley, J.H. Burroughes, R.H. Friend, N.C. Greenham, P.L. Burns, A.B. Holmes, A. Kraft: Appl. Phys. Lett. **61**, 2793 (1992)
5. X. Jiang, Y. Liu, X. Song, D. Zhu: Solid State Commun. **99**, 183 (1996)
6. R. Antony, B. Ratier, A. Moliton: Opt. Mater. **12**, 291 (1999)
7. B.G. Bovard: In *Thin Films for Optical systems*, ed. by F.R. Flory (Marcel Dekker, New York 1995) p. 117
8. R. Antony, A. Moliton, B. Ratier, C. Moussant: Eur. Phys. J. AP. **4**, 45 (1998)
9. A. Schmidt, M.L. Anderson, N.R. Armstrong: J. Appl. Phys. **78**, 5619 (1995)
10. P.E. Burrows, Z. Shen, V. Bulovic, D.M. McCarty, S.R. Forrest, J.A. Cronin, M.E. Thompson: J. Appl. Phys. **79**, 7991 (1996)
11. P. Varga, U. Diebold: In *Low-energy Ion – Surface Interactions*, ed by J.W. Rabalais (Wiley, New York 1994) Chapt. 7
12. W.H. Holber: In *Handbook of Ion beam Processing Technology*, ed. by J.J. Cuomo, S.M. Rossnagel, H.R. Kaufman (Noyes 1989) Chapt. 3
13. A. Moliton: ANVAR industrial contract, n°9203022K (1996)
14. F.A. Smidt: Int. Mater. Rev. **35**, 61 (1990)
15. J.F. Ziegler: In *Handbook of Ion Implantation Technology*, ed. by J.F. Ziegler (Elsevier, Amsterdam 1992)
16. W. Eckstein: *Computer Simulation of Ion-Solid Interactions* (Springer, Berlin, Heidelberg 1991) p. 26

17. M.T. Robinson, I.M. Torrens: Phys. Rev. B **9**, 5008 (1974)
18. R. Antony, A. Moliton, B. Ratier: J. Chim. Phys. **95**, 586 (1998)
19. J. Kyokane, I. Taniguchi, K. Yoshino: Synth. Met. **71**, 2219 (1995)
20. J. Kyokane, R. Aoyagi, K. Yoshino: Synth. Met. **85**, 1393 (1997)
21. B.A. Movchan, A.V. Denchishin: Fiz. Met. Metalloved. **28**, 653 (1969)
22. J.A. Thornton: J. Vac. Sci. Technol. **11**, 666 (1974)
23. K.H. Muller: In *Handbook of Ion-beam Processing Technology*, ed. by J.J. Cuomo et al. (Noyes 1989) Chapt. 13
24. E. Kay, S.M. Rossnagel: *Handbook of Ion-beam Processing Technology*, ed. by J.J. Cuomo et al. (Noyes 1989) p. 184
25. P.J. Hamer, K. Pichler, M.G. Harisson, R.H. Friend, B. Ratier, A. Moliton, S.C. Moratti, A.B. Holmes: Philos. Mag. B **73**(2), 367 (1996)
26. T. Venkatesan, L. Calcagno, B.S. Elman, G. Fotti: In *Ion-beam Modification of Insulators*, ed. by P. Mazzoldi, G.W. Arnold (Elsevier, Amsterdam 1987)
27. A. Moliton: In *Handbook of Conducting Polymers*, 2nd edn., ed. by R. Elsenbaumer, J.R. Reynolds, T. Skotheim (Marcel Dekker, New York 1997) Chapt. 21
28. J. Bell: Opto Laser Europe **60**, 21 (1999)
29. A. Moliton, B. Lucas, C. Moreau, R.H. Friend: Philos. Mag. B **69**(6), 1155 (1994)
30. T. Mori, T. Mizutani: Polym. Adv. Technol. **8**, 471 (1997)
31. A. Kraft, A.C. Grimsdale, A. Holmes: Angew. Chem. Int. Ed. **37**, 402 (1998)
32. R. Antony: Thèse n°22 – 1998, Université de Limoges
33. T.P. Nguyen, P. Jolinat, P. Destruel, R. Clergereaux, J. Farenc: Thin Solid Films, in press